



ISTITUTO NAZIONALE DI RICERCA METROLOGICA Repository Istituzionale

Efficient prediction of MRI gradient-induced heating for guiding safety testing of conductive implants

Original

Efficient prediction of MRI gradient-induced heating for guiding safety testing of conductive implants / Zanovello, Umberto; Fuss, Carina; Arduino, Alessandro; Bottauscio, Oriano. - In: MAGNETIC RESONANCE IN MEDICINE. - ISSN 0740-3194. - 90:5(2023), pp. 2011-2018. [10.1002/mrm.29787]

Availability:

This version is available at: 11696/78019 since: 2023-10-27T07:55:12Z

Publisher:

WILEY

Published

DOI:10.1002/mrm.29787

Terms of use:

This article is made available under terms and conditions as specified in the corresponding bibliographic description in the repository

Publisher copyright

(Article begins on next page)

Efficient prediction of MRI gradient-induced heating for guiding safety testing of conductive implants

Umberto Zanovello¹  | Carina Fuss²  | Alessandro Arduino¹  | Oriano Bottauscio¹ 

¹Metrologia dei materiali innovativi e scienze della vita, Istituto Nazionale di Ricerca Metrologica, Torino, Italy

²IT²IS Foundation, Zurich, Switzerland

Correspondence

Umberto Zanovello, Metrologia dei materiali innovativi e scienze della vita, Istituto Nazionale di Ricerca Metrologica, Strada delle Cacce 91, 10035 Torino, Italy.
Email: u.zanovello@inrim.it

Funding information

European Association of National Metrology Institutes, Grant/Award Number: 21NRM05 STASIS

Abstract

Purpose: To propose an efficient numerical method to predict the temperature increase of an implantable medical device induced by any linearly polarized homogeneous magnetic field, according to the ISO 10974 methodology for testing of gradient-induced device heating.

Theory and Methods: The concepts of device-specific power and temperature tensors are introduced to mathematically describe the electromagnetic and thermal anisotropic behavior of the device, from which the device heating for an arbitrary exposure direction can be predicted. The proposed method is compared to a brute-force approach based on simulations, and validated by applying it to four reference orthopedic implants with a commercial simulation software.

Results: The proposed method requires about 5% of the time required by the brute-force approach, and 30% of the memory occupancy. The temperature increase predicted by the proposed method over a range of incident magnetic field exposures deviated from brute-force direct simulations by less than $\pm 0.3\%$.

Conclusion: The proposed method allows efficient prediction of the heating of an implantable medical device induced by any linearly polarized homogeneous magnetic field using a small fraction of the simulations required by the brute-force approach. The results can be used to predict the worst-case orientation of the gradient field, for subsequent experimental characterization according to the ISO 10974 standard.

KEYWORDS

gradient-induced heating, implant testing, ISO 10974, MRI safety, numerical simulations

1 | INTRODUCTION

MRI is a largely used imaging tool for noninvasive clinical diagnosis. Despite significant efforts in making MRI an increasingly safe technique, many safety issues are still being addressed, especially when it comes to patients carrying implantable medical devices.¹⁻⁵ This is of particular

concern due to the growing number of implanted orthopedic devices⁶⁻⁹ and the related need of MRI examinations aimed at assessing possible perioperative and postoperative complications.¹⁰

One main safety issue in this regard is MRI-induced heating of the tissues surrounding the implant. Radiofrequency (RF) tissue heating has gained a wide

This is an open access article under the terms of the [Creative Commons Attribution](https://creativecommons.org/licenses/by/4.0/) License, which permits use, distribution and reproduction in any medium, provided the original work is properly cited.

© 2023 The Authors. *Magnetic Resonance in Medicine* published by Wiley Periodicals LLC on behalf of International Society for Magnetic Resonance in Medicine.

attention both from the literature and relevant standards due to its potential to cause significant temperature increases when the incident RF field, implant characteristics, and exposure scenario meet specific criteria.^{11–17} While RF remains the most important source of heating in MRI, recent studies showed that heating induced by gradient fields could also represent a risk in the presence of bulky conductive objects.^{5,18,19}

The ISO 10974 standard¹⁷ recognizes that the switching gradient fields can induce significant electric currents on an active implantable medical device enclosure. Such currents lead to heating of the device, with a consequent risk for the patient. For this reason, the standard proposes a specific test to experimentally assess the gradient heating risk. During the test, the active implantable medical device is exposed to a linearly polarized harmonic homogeneous magnetic field oriented along the direction which maximizes the heating. The maximum temperature increase on the active implantable medical device enclosure is then measured after a suggested time of 30 min of ongoing exposure. While the worst exposure direction in terms of heating can be identified rather easily for a disk-like active implantable medical device enclosure, it may be difficult to be identified when the same test is performed on objects with a more complex shape, such as many orthopedic implants.²⁰ In this case, the worst exposure direction has to be investigated through several different experiments where, in each experiment, the orientation of the device under test (DUT) is slightly changed and the temperature increase is recorded and compared with those obtained with the other orientations. While recording the temperature increase for all possible device orientations and all over its surface is not feasible, reducing the number of tested orientations and recording points does not assure that the worst device orientation and maximum temperature increase are properly identified. In this context, demonstrating compliance with MRI safety regulations and obtaining “MR conditional” labeling becomes even more challenging and expensive for implant manufacturers and testing companies.²¹

Numerical simulations provide a valuable tool to address this issue whenever the virtual model of the DUT is available. However, approaching the problem through a brute-force strategy is still far from an efficient solution. Indeed, a large number of simulations is required to reliably identify the worst-case direction, costing significant computational time as well as storage of result files.^{20,22}

In this paper, we propose a strategy to predict the gradient-induced heating of any passive implant under any linearly-polarized homogeneous magnetic field by performing a minimum amount of numerical simulations to generate a number of 3×3 tensors which characterize the implant response. We validated the method through

a comparison with a set of explicit gradient heating simulations representing a brute-force approach. We performed all simulations in Sim4Life,²³ and developed a Python script that can be used in Sim4Life to automatically compute the worst exposure direction after the virtual model of an implant is imported. The script is available in the authors' GitHub repository²⁴ along with basic documentation and a relevant example.

2 | THEORY

2.1 | Power tensor

The current density $\mathbf{j}(\mathbf{x})$ generated in a spatial point \mathbf{x} of the DUT by a linearly polarized harmonic homogeneous magnetic flux density \mathbf{B} can be defined as

$$\mathbf{j}(\mathbf{x}) = \sum_{i=1}^3 \mathbf{j}_i^u(\mathbf{x}) B_i = \mathbf{J}(\mathbf{x}) \mathbf{B}, \quad (1)$$

where $\mathbf{j}_i^u(\mathbf{x})$ is a three element complex vector representing the (peak) harmonic current density generated in \mathbf{x} by a unitary magnetic flux density oriented along the i th Cartesian direction and with the same frequency of \mathbf{B} , B_i is the i th component of the magnetic flux density \mathbf{B} and $\mathbf{J}(\mathbf{x})$ is a 3×3 matrix with the $\mathbf{j}_i^u(\mathbf{x})$ vectors as columns. Since \mathbf{B} is linearly polarized, we can assume that $\mathbf{B} \in \mathbb{R}^3$.

The local power density $p(\mathbf{x})$ dissipated in \mathbf{x} by the Joule losses can be computed as

$$p(\mathbf{x}) = \Re \left[\frac{1}{2\sigma} \mathbf{j}(\mathbf{x})^H \mathbf{j}(\mathbf{x}) \right] = \frac{1}{2\sigma} \mathbf{B}^T \Re [\mathbf{J}(\mathbf{x})^H \mathbf{J}(\mathbf{x})] \mathbf{B}, \quad (2)$$

where σ is the electrical conductivity in \mathbf{x} , \Re denotes the real part, and T and H superscripts denote the transpose and Hermitian transpose operators, respectively. The total power P deposited inside the DUT is obtained by integrating (2) over the DUT volume (\mathcal{V}) as

$$P = \int_{\mathcal{V}} p(\mathbf{x}) d\mathbf{x} = \mathbf{B}^T \int_{\mathcal{V}} \frac{1}{2\sigma} \Re [\mathbf{J}(\mathbf{x})^H \mathbf{J}(\mathbf{x})] d\mathbf{x} \mathbf{B} = \mathbf{B}^T \mathbf{Q} \mathbf{B}. \quad (3)$$

Here, \mathbf{Q} is a device-specific 3×3 positive semidefinite symmetric tensor which relates the power deposited inside the DUT to the linearly polarized harmonic homogeneous magnetic flux density which is responsible for the power deposition. The tensor \mathbf{Q} can be computed by means of three electromagnetic simulations aiming at obtaining the current densities $\mathbf{j}_i^u(\mathbf{x})$.

The tensor \mathbf{Q} describes the anisotropy of the DUT with respect to the electromagnetic problem.

2.2 | Temperature tensor field

Since the power density distribution inside the DUT and the resulting temperature increase are proportional in a phantom experiment, it is possible to express the latter with a quadratic form similar to that obtained for the power deposition. From (2), it is possible to express the temperature rise in each voxel of the implant as

$$\Delta T(\mathbf{x}) = \mathcal{L}_T[p](\mathbf{x}) = \mathbf{B}^T \mathbf{M}(\mathbf{x}) \mathbf{B}, \quad (4)$$

where \mathcal{L}_T is the linear operator solving the heat equation,

$$\rho c_p \frac{\partial u}{\partial t} - \nabla \cdot (\lambda \nabla u) = p.$$

Therefore, \mathcal{L}_T depends on the thermal conductivity λ , the mass density ρ and the specific heat capacity c_p of the DUT and the surrounding environment. The linearity of \mathcal{L}_T allows introducing $\mathbf{M}(\mathbf{x})$, device-specific 3×3 positive semidefinite symmetric tensors which relate the temperature increase in any spatial point \mathbf{x} of the DUT with the linearly polarized harmonic homogeneous magnetic field responsible for it. While the tensor \mathbf{Q} alone represents the whole DUT with regard to power deposition, the temperature is not a global quantity, and the implant is characterized by a tensor field, where each $\mathbf{M}(\mathbf{x})$ tensor is relevant to the temperature increase at a specific position in the DUT. Considering that the tensors $\mathbf{M}(\mathbf{x})$ are symmetric, the whole tensor field can be computed with six thermal simulations. Indeed, the m, n component of $\mathbf{M}(\mathbf{x})$ is equal to the temperature rise distribution following the application of a fictitious power density

$$p_{m,n}(\mathbf{x}) = \frac{1}{2\sigma} \Re \left[(\mathbf{j}_n^u)^H \mathbf{j}_m^u \right].$$

The tensor $\mathbf{M}(\mathbf{x})$ describes the anisotropy of the DUT in \mathbf{x} with respect to the complete (electromagnetic and thermal) problem.

2.3 | Worst exposure orientation

With reference to the quadratic form in (3), the maximum power deposition inside the DUT following the application of a linearly polarized unitary harmonic homogeneous magnetic flux density is given by the largest eigenvalue of \mathbf{Q} . The maximum power deposition is obtained with a magnetic flux density oriented as an eigenvector associated with the largest eigenvalue (see Appendix S1). Similarly, the maximum temperature increase in a DUT point \mathbf{x} is given by the largest eigenvalue of $\mathbf{M}(\mathbf{x})$ and it is induced by a magnetic flux density oriented as one of the corresponding eigenvectors. The overall maximum temperature increase in the DUT and the relevant magnetic flux density direction can be retrieved by identifying the maximum among the maximum eigenvalues of the $\mathbf{M}(\mathbf{x})$ tensors.

3 | METHODS

The above procedure was implemented in Sim4Life²³ and applied on four orthopedic implants, described in Table 1, in order to identify the exposure conditions that maximize the power deposition and the temperature increase. To validate the method, the deposited power and the resulting maximum temperature increase of the shoulder implant were computed in Sim4Life, by exposing the implant to a homogeneous magnetic flux density with amplitude equal to 35 mT and frequency equal to 270 Hz (i.e., the values proposed in ISO 10974¹⁷) while varying the magnetic flux density direction to cover the surface of a hemisphere with angular steps of 22.5°. After that, the \mathbf{Q} and $\mathbf{M}(\mathbf{x})$ tensors were computed and, for each magnetic flux density direction, the power deposited into the shoulder implant and the maximum temperature increase previously obtained were compared to the same quantities computed according to (3) and (4). Eventually, the worst exposure orientation

TABLE 1 List of the simulated orthopedic implants together with their properties.

| Implant | Manufacturer | Materials | Description |
|-------------|---------------|--|---|
| Shoulder | LimaCorporate | Ti6Al4V | Partial anatomical shoulder arthroplasty with 44 mm humeral head diameter and 103 mm humeral stem length. |
| Hip | Adler Ortho | Sphere: CoCrMo, Acetabular cup & Stem: Ti6Al4V, Liner: UHMW-PE | Total hip arthroplasty with 52 mm acetabular cup diameter, 135 mm stem length and 32 mm sphere diameter. |
| Knee | Adler Ortho | Tibial & Femoral components: CoCrMo, Liner: UHMW-PE | Bi-compartmental knee arthroplasty with femoral component dimensions 53 mm × 63 mm × 46 mm and tibial component dimensions 47 mm × 73 mm × 35 mm. |
| Ankle Plate | Medartis AG | Ti6Al4V | Medial, distal tibia plate 260 mm long. |

deduced by the proposed method, and the corresponding result, were compared to those obtained by the brute-force approach.

To comply with the requirements of ISO 10974,¹⁷ the thermal simulations, required to compute the $\mathbf{M}(\mathbf{x})$ tensor field, were performed with the implants centrally positioned inside a phantom. The dimensions of the phantom ($130\text{ mm} \times 200\text{ mm} \times 400\text{ mm}$) guaranteed that the phantom-air boundary conditions did not play a significant role in the thermal results for the 30min simulated thermal evolution (see Figure S1). The thermal properties of the phantom (specific heat capacity: $4150\text{ J kg}^{-1}\text{ K}^{-1}$, thermal conductivity: $0.54\text{ W m}^{-1}\text{ K}^{-1}$) complied with those reported in the ASTM standard¹⁶ for the polyacrylic acid-based solution. The phantom was not included in the electromagnetic simulations performed to

compute the \mathbf{Q} tensor, since its low electrical conductivity (with respect to that of the conductive implants) would not significantly affect the deposited power.²⁵ All simulations were performed using an isotropic 1 mm^3 mesh on an Intel(R) Xeon(R) E5-2650 CPU with 64 GB of RAM.

4 | RESULTS

The validation of the proposed method is illustrated in Figure 1, where the power deposited inside the shoulder implant and the maximum temperature increase are compared for 60 different magnetic flux density orientations. The results are reported describing the exposure orientation according to the Cartesian system represented in the bottom-right corner of the figure where θ is the polar angle

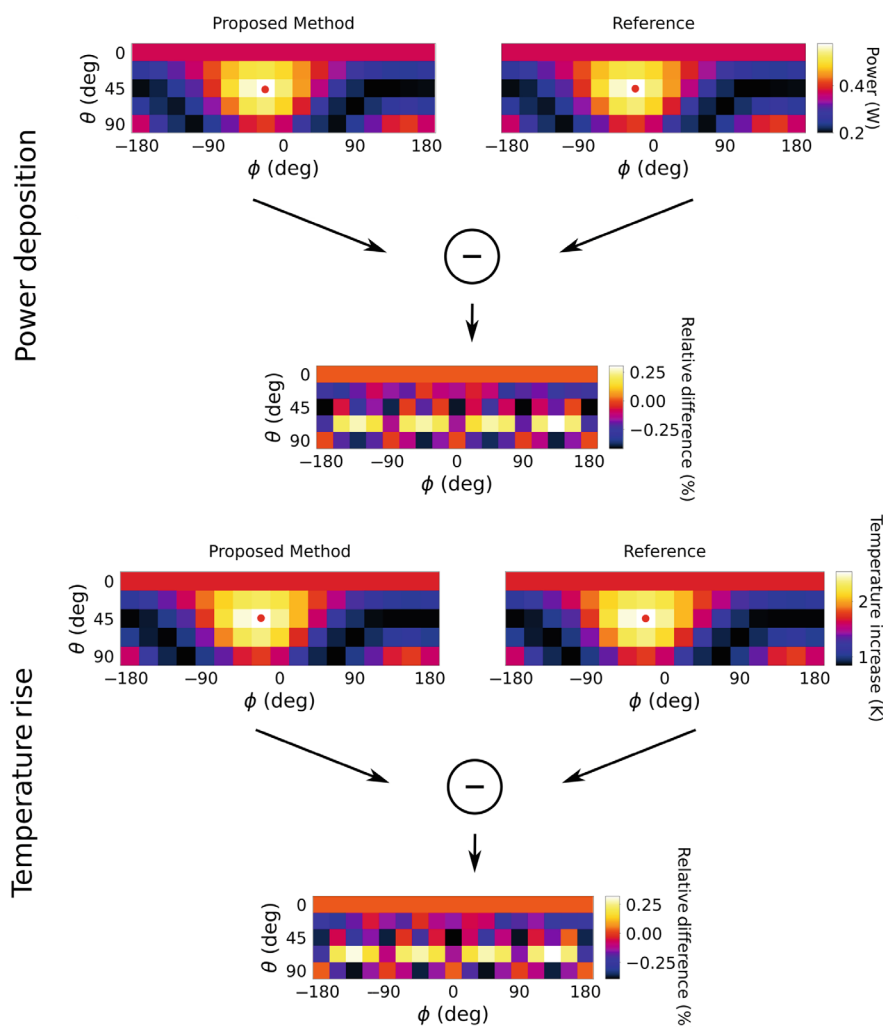


FIGURE 1 Deposited power and maximum temperature rise values obtained with the proposed method compared to those obtained through reference brute-force simulations. The results for the shoulder implant exposed to a 270 Hz magnetic flux density with 35 mT intensity are shown. θ represents the polar angle and ϕ the azimuth angle. The θ and ϕ angles leading to the maximum power deposition and temperature increase ($\theta = 45^\circ$ and $\phi = -22.5^\circ$, in both cases) are identified by the red dots in the color maps.

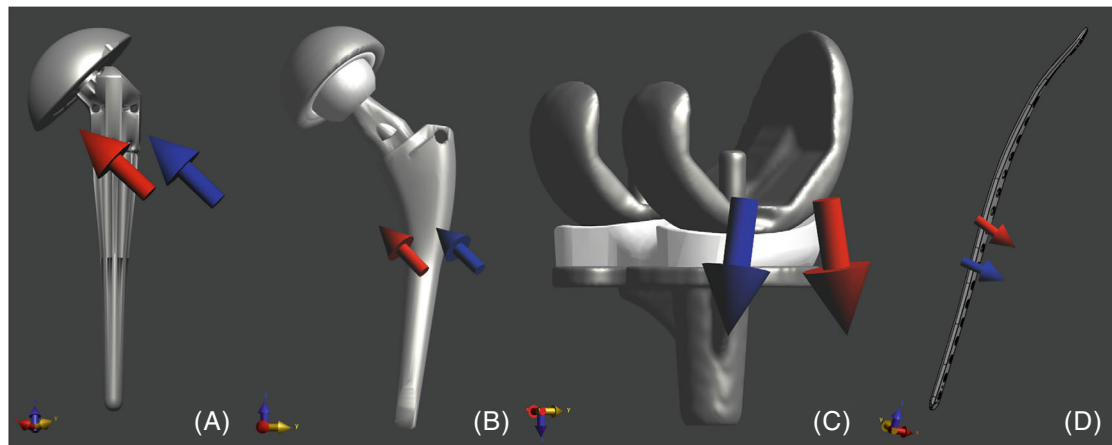


FIGURE 2 Orientation of the magnetic flux density which maximizes the power deposition (blue) and the peak temperature increase after 30-min of exposure (red). Results are shown for the shoulder implant (A), hip implant (B), knee implant (C), and ankle plate (D).

and ϕ the azimuth angle. The results reveal a maximum difference between the simulated power depositions and those computed through the tensor \mathbf{Q} of about $\pm 0.3\%$. The same difference is obtained looking at the maximum temperature increases after 30-min exposure.

Figure 2 represents, for each implant, the worst exposure orientations, estimated with the proposed approach, which maximize the power deposition inside the implant (blue arrow) and the peak temperature increase after 30-min of exposure (red arrow).

The first row of Figure 3 shows the maximum temperature increase that each voxel of the implants can reach when exposed to a homogeneous magnetic flux density of 35 mT at 270 Hz. The second row of Figure 3 shows the distributions of the temperature increase induced in each implant exposed to the homogeneous magnetic flux density of 35 mT at 270 Hz oriented along the direction which maximizes the peak temperature increase within the implant.

The orientation of the magnetic flux density which results in maximum temperature increase at each point is illustrated in Figure 4. The arrow colors correspond to those in the second row of Figure 3.

5 | DISCUSSION

The negligible difference in power and peak temperature estimates between the brute-force approach and the proposed method demonstrates the reliability of the proposed procedure. In order to compute the $\mathbf{M}(\mathbf{x})$ tensor field, the computations required about 4 h to perform the three electromagnetic and six thermal simulations, yielding 4.5 GB of data. The brute-force approach required almost 80 h of computations in order to perform the 60 electromagnetic and thermal simulations, producing 13.4 GB of data (noting that both times could have been further shortened by

enabling GPU acceleration). Finally, the proposed method determines the actual maximum power deposition and peak temperature increase.

With a 22.5° angular step, the brute-force approach, used for validating the proposed method, estimates a maximum power deposition of 0.577 W and a maximum temperature increase of 2.53 K. In both cases, these values are obtained for magnetic flux density oriented according to $\theta = 45^\circ$ and $\phi = -22.5^\circ$. The proposed procedure computes a maximum power deposition of 0.582 W (for $\theta = 47.41^\circ$ and $\phi = -27.46^\circ$) and a maximum temperature increase of 2.54 K (for $\theta = 47.28^\circ$ and $\phi = -30.46^\circ$). In this case, the brute-force approach revealed to be reliable but this may not be the case in general. In fact, the discretization of the magnetic flux density direction sweep could lead to an underestimation of the above quantities if an inadequate discretization step is selected.

The magnetic flux density directions which maximize the power deposition and the peak temperature increase are slightly different (Figure 2), especially for the knee implant (Figure 2C) and the ankle plate (Figure 2D). Looking at the angle formed by the two magnetic flux density directions, we obtain a very good direction coherence for the shoulder and hip implants (3.89° and 8.39° , respectively) and a slightly worse coherence for the knee implant and the ankle plate (15.55° and 15.5° , respectively). The relative difference between the maximum peak temperature increases and those resulting from the exposition of the implant to a homogeneous magnetic flux density oriented according the direction which maximize the power deposition are equal to 0.8% for the shoulder implant, 1.27% for the hip implant, 3.7% for the knee implant and 5.85% for the ankle plate.

Figure 3 shows that, while there is a direction of the magnetic flux density which maximizes the peak temperature increase within the implant, peak temperatures close

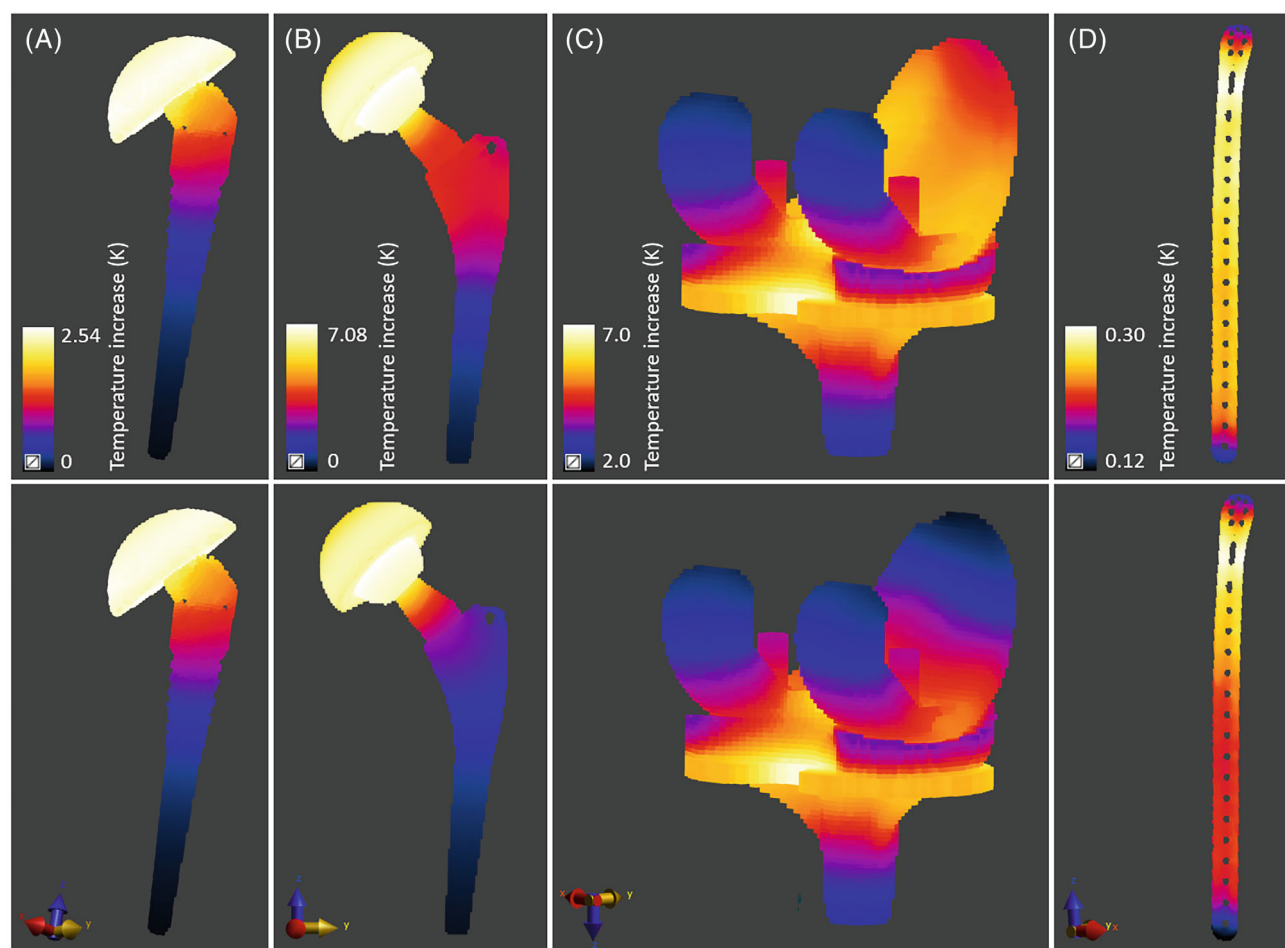


FIGURE 3 First row: Chromatic maps representing, in each voxel, the temperature increase following the exposure to the homogeneous magnetic flux density whose direction maximizes the temperature increase in the same voxel. Second row: Temperature increase distributions resulting from the exposure to the homogeneous magnetic flux density whose direction maximizes the peak temperature increase in the implant. Results are shown for the shoulder implant (A), hip implant (B), knee implant (C), and ankle plate (D). All temperature increases are after 30 min of exposure to a 35 mT magnetic flux density with a 270 Hz frequency.

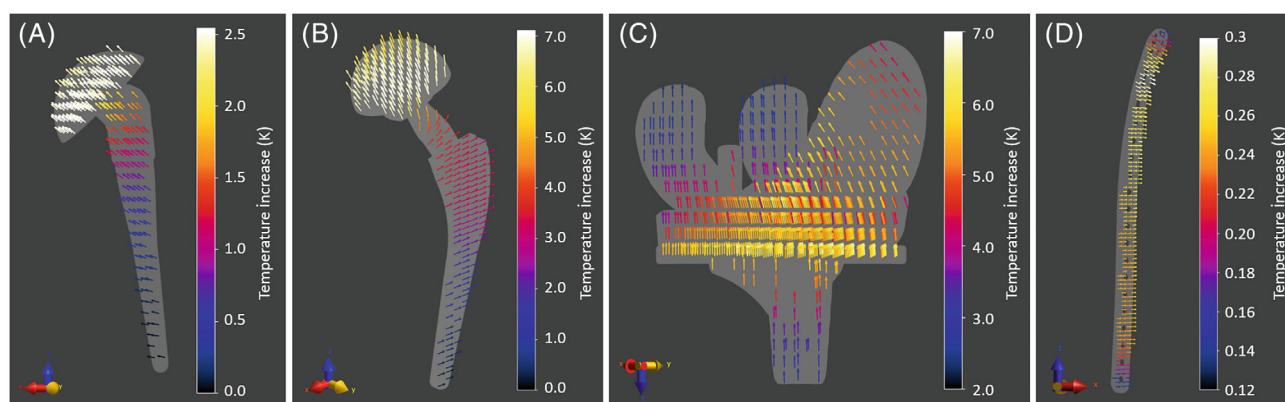


FIGURE 4 Vector field plots representing the direction of the magnetic flux density which maximizes the temperature increase at the arrow position. The arrow colors correspond to those in the second row of Figure 3. Results are shown for the shoulder implant (A), hip implant (B), knee implant (C), and ankle plate (D).

to the maximum value can be attained by significantly different directions (see also Figure 4). This is particularly true for the knee implant (Figure 3C) and the ankle plate (Figure 3D). Dealing with the knee implant exposed to the magnetic flux density oriented along the worst direction (bottom row), the femoral component shows a temperature rise much lower than that encountered on the tibial component. However, the top row of Figure 3C shows that the femoral component can heat up quite as much as the tibial component for certain magnetic flux density directions. The ankle plate is seen to behave similarly when comparing the top and bottom rows of Figure 3D.

This information can help to define the position of the temperature probes in the ISO 10974 experiment and, combining the information contained in Figure 4, to identify further implant orientations to be tested for backup experiments. Indeed, if the digital model of the implant differs from the physical model, the point-wise worst possible temperature increase (second row of Figure 3) indicates locations which could be sensitive to variation.

Regarding the skin effect: the Sim4Life magneto quasi-static solver, used to compute the \mathbf{Q} matrix, solves the Maxwell equations neglecting the reaction due to the eddy-currents induced into the conductive components of the implant. By comparison with a homemade code,^{26,27} we found that the skin effect does not play a significant role for the considered implants at 270 Hz. However, this would have to be rechecked for higher test frequencies, such as the 1750 Hz proposed in the latest draft edition of ISO 10974.²⁰

Another direct consequence of the low frequency value is that the power deposited into the phantom is negligible with respect to that into the conductive implant. This behavior is typical for gradient coil-induced heating which sensibly differs from RF induced heating where the majority of the power is deposited into the tissues surrounding the implant.^{5,25} This allowed us to save some disk space by removing the phantom in the electromagnetic simulations after verifying, for a selected case, that the results were not affected.

Finally, the proposed method allows to easily calculate the implant-related anisotropy coefficients proposed by Arduino et al.,²² used to avoid over-conservative safety limits when dealing with gradient-induced heating of implantable medical devices.

6 | CONCLUSION

We have presented a numerical method to efficiently predict the power deposition and temperature increase inside a conductive medical implant experiencing a linearly polarized harmonic homogeneous magnetic flux density. The proposed strategy reduces the efforts and

time required to perform gradient-heating measurements of passive medical implants following the ISO 10974 test methodology, compared to a brute-force approach.

The proposed method has been implemented in Sim4Life, successfully validated, and applied to four orthopedic implants. A Sim4Life Python script that implements the method and automatically computes the orientations that maximize the deposited power and the induced temperature increase is provided in the authors' GitHub repository.²⁴ The script also provides functions for visualizing the results, and it is provided together with basic documentation and a usage example.

ACKNOWLEDGMENTS

The project (21NRM05 STASIS) has received funding from the European Partnership on Metrology, co-financed from the European Union's Horizon Europe Research and Innovation Programme and by the Participating States. Hip, knee and shoulder implants and related digital models have been kindly provided by Laboratorio di Tecnologia Medica, IRCCS Istituto Ortopedico Rizzoli, Bologna, Italy. The ankle plate and related digital model has been kindly provided by Medartis AG. The authors sincerely thank Dr. Tolga Goren and Dr. Lena Kranold for the valuable discussions and the contributions provided for the language editing of the paper.


CONFLICT OF INTEREST STATEMENT

The authors declare no potential conflict of interests.

ORCID

Umberto Zanovello  <https://orcid.org/0000-0001-6415-9967>

Carina Fuss  <https://orcid.org/0009-0007-5629-9290>

Alessandro Arduino  <https://orcid.org/0000-0002-4829-5130>

Oriano Bottauscio  <https://orcid.org/0000-0002-5437-4396>

REFERENCES

1. Winter L, Seifert F, Zilberti L, Murbach M, Ittermann B. MRI-related heating of implants and devices: a review. *J Magn Reson Imaging*. 2021;53:1646-1665.
2. Murbach M, Zastrow E, Neufeld E, Cabot E, Kainz W, Kuster N. Heating and safety concerns of the radio-frequency field in MRI. *Curr Radiol Rep*. 2015;3:45.
3. Yao A, Goren T, Samaras T, Kuster N, Kainz W. Radiofrequency-induced heating of broken and abandoned implant leads during magnetic resonance examinations. *Magn Reson Med*. 2021;86:2156-2164.
4. Yao A, Murbach M, Goren T, Zastrow E, Kainz W, Kuster N. Induced radiofrequency fields in patients undergoing MR examinations: insights for risk assessment. *Phys Med Biol*. 2021;66:185014.

5. Arduino A, Zanovello U, Hand J, et al. Heating of hip joint implants in MRI: the combined effect of RF and switched-gradient fields. *Magn Reson Med*. 2021;85:3447-3462.
6. Lübbecke A, Silman AJ, Barea C, Prieto-Alhambra D, Carr AJ. Mapping existing hip and knee replacement registries in Europe. *Health Policy*. 2018;122:548-557.
7. Mond HG, Crozier I. The Australian and New Zealand cardiac implantable electronic device survey: calendar year 2017. *Heart Lung Circ*. 2019;28:560-566.
8. Zecchin M, Torre M, Carrani E, et al. Seventeen-year trend (2001–2017) in pacemaker and implantable cardioverter-defibrillator utilization based on hospital discharge database data: an analysis by age groups. *Eur J Intern Med*. 2021;84:38-45.
9. Kurtz SM, Ochoa JA, Lau E, et al. Implantation trends and patient profiles for pacemakers and implantable cardioverter defibrillators in the United States: 1993–2006. *Pacing Clin Electrophysiol*. 2010;33:705-711.
10. Gallo J, Kamínek P, Tichá V, Řiháková P, Ditmar R. Particle disease. A comprehensive theory of periprosthetic osteolysis: a review. *BIOMED PAP*. 2002;146:21-28.
11. Stenschke J, Li D, Thomann M, Schaefer G, Zylka W. A numerical investigation of RF heating effects on implants during MRI compared to experimental measurements. *Advances in Medical Engineering*. Springer; 2007:53-58.
12. Song T, Xu Z, Iacono MI, Angelone LM, Rajan S. Retrospective analysis of RF heating measurements of passive medical implants. *Magn Reson Med*. 2018;80:2726-2730.
13. Nordbeck P, Fidler F, Weiss I, et al. Spatial distribution of RF-induced E-fields and implant heating in MRI. *Magn Reson Med*. 2008;60:312-319.
14. Wooldridge J, Arduino A, Zilberti L, et al. Gradient coil and radiofrequency induced heating of orthopaedic implants in MRI: influencing factors. *Phys Med Biol*. 2021;66:245024.
15. International Electrotechnical Commission (IEC). *Medical Electrical Equipment - Part 2-33: Particular Requirements for the Basic Safety and Essential Performance of Magnetic Resonance Equipment for Medical Diagnosis*. Standard IEC 60601-2-33:2022. International Electrotechnical Commission (IEC); 2022.
16. American Society for Testing and Materials (ASTM). *Standard Test Method for Measurement of Radio Frequency Induced Heating on or near Passive Implants during Magnetic Resonance Imaging*. Standard F2182-19. American Society for Testing and Materials (ASTM); 2019.
17. International Organization for Standardization (ISO). *Assessment of the Safety of Magnetic Resonance Imaging for Patients with an Active Implantable Medical Device*. Standard ISO/TS 10974. International Organization for Standardization (ISO); 2018.
18. Clementi V, Zanovello U, Arduino A, et al. Classification scheme of heating risk during MRI scans on patients with orthopaedic prostheses. *Diagnostics*. 2022;12:1873.
19. Brühl R, Ihlenfeld A, Ittermann B. Gradient heating of bulk metallic implants can be a safety concern in MRI. *Magn Reson Med*. 2017;77:1739-1740.
20. Bassen H, Zaidi T. Parameters affecting worst-case gradient-field heating of passive conductive implants. *J Magn Reson Imaging*. 2022;56:1197-1204.
21. Center for Devices and Radiological Health. *Testing and Labeling Medical Devices for Safety in the Magnetic Resonance (MR) Environment. Guidance for Industry and Food and Drug Administration Staff*. Standard. U.S. Food & Drug, Center for Devices and Radiological Health Silver Spring; 2021.
22. Arduino A, Bottauscio O, Chiampi M, Zanovello U, Zilberti L. A contribution to MRI safety testing related to gradient-induced heating of medical devices. *Magn Reson Med*. 2022;88:930-944.
23. Zurich Med Tech. Sim4Life. Accessed June 23, 2023. <https://zmt.swiss/sim4life>
24. Umberto Z, Carina F, Alessandro A, Oriano B. Sim4Life, Worst Orientation Python script. 2023. Accessed June 23, 2023. https://github.com/umbertozanovello/sim4life_GC_WorstOrientation
25. Arduino A, Baruffaldi F, Bottauscio O, et al. Computational dosimetry in MRI in presence of hip, knee or shoulder implants: do we need accurate surgery models? *Phys Med Biol*. 2022;67:245022.
26. Bottauscio O, Chiampi M, Hand J, Zilberti L. A GPU computational code for Eddy-current problems in voxel-based anatomy. *IEEE Trans Magn*. 2015;51:1-4.
27. Alessandro A, Oriano B, Mario C, Luca Z. Douglas–Gunn method applied to dosimetric assessment in magnetic resonance imaging. *IEEE Trans Magn*. 2017;53:5000204.

SUPPORTING INFORMATION

Additional supporting information may be found in the online version of the article at the publisher's website.

Appendix S1. Quadratic Form maximisation Figure S1: Maximum temperature rises as a function of the distance from the phantom centre for the four analysed implants. The temperature rises are obtained after 1800 s of exposure to the magnetic flux density oriented along the direction that maximizes the peak temperature increase. Eachline represents the maximum temperature rise on the planes orthogonal to that line. In order to represent the three lines in the same panel, the distance from the phantom centre is normalised with respect to the phantom dimension along the relevant line direction. The maximum temperature rises approach zero at the y and z phantom boundaries. A slight temperature increase is appreciable at the x boundary of the phantom. The dimension of the phantom along the x direction is indeed shorter (130 mm) with respect to the y and z dimensions (200 mm and 400 mm, respectively). Nevertheless, the temperature rise at the phantom boundaries is always below the 4.5 % of the peak temperature increase in the implant, with an only exception for the knee implant where it reaches the 7.5 %

How to cite this article: Zanovello U, Fuss C, Arduino A, Bottauscio O. Efficient prediction of MRI gradient-induced heating for guiding safety testing of conductive implants. *Magn Reson Med*. 2023;90:2011-2018. doi: 10.1002/mrm.29787